Tunable Single-Polarization Single-Mode Microstructured Polymer Optical Fiber

Yovanny A. V. Espinel, Marcos A. R. Franco, and Cristiano M. B. Cordeiro

***Abstract*—A new procedure to obtain single-polarization single-mode polymeric optical fibers is reported. The selective polarization confinement loss mechanism is obtained by applying external hydrostatic pressure in a specially designed side-hole microstructured polymer optical fiber. It is shown that, at $\lambda = 588$ nm, pressure around 380 bar allows inducing confinement loss as high as 35 dB/m for one polarization state while the other is guided with low loss (3×10^{-3} dB/m). The loss mechanism is shown to be related to coupling between the fundamental core modes and the cladding modes of the pressurized fiber. Finally, the possibility of tuning the single-polarization single-mode state with the input wavelength with fixed pressure or by introducing small changes in the inner ring of holes of the fiber cross section is presented.**

***Index Terms*—Confinement loss, fundamental space-filling modes (FSMs), microstructured polymer optical fiber, photoelastic effect, single polarization.**

I. Introduction

SINCE THE appearance of photonic crystal fibers, new and exciting applications have been developed due to their remarkable propagation characteristics [1]–[3]. Taking advantage of these features, many theoretical and experimental studies are being realized relating some propagation characteristics of the fibers, made of silica or polymethylmethacrylate (PMMA), and its external conditions such as hydrostatic pressure, temperature, strain, or bending [4]–[8]. For instance, in the case of temperature, it was found that phase modal birefringence sensitivity is at least one order of magnitude smaller in photonic crystal fibers than in conventional birefringence optical fibers. This feature has strongly motivated the use of microstructured optical fibers in sensors of other physical quantities such as pressure, axial force, and strain.

When hydrostatic pressure is applied on the fiber, the phase modal birefringence and confinement loss are modified due to the photoelastic effect. In the first case, it is possible to make interferometric modal sensors [5]. Playing with the confinement loss, on the other hand, makes it possible to reach a single-polarization single-mode (SPSM) state with some fiber geometries [9]–[12]. These SPSM fibers are useful as polarizing elements in high-power fiber lasers, fiber optic gyroscopes, current sensors, and super luminescent sources [13]. An SPSM microstructured polymer optical fiber (mPOF) was already reported as a potential candidate for applications in ultrahigh-speed data transmissions in short distance local area networks [11]. This application also opens the possibility to use mPOFs in areas related to Fibre To The Home, automotive industry, and consumer electronics where the standard polymer optical fibers are already in use [3].

To reach the single polarization state, the present authors showed recently a brief study relating the influence of hydrostatic pressure over the confinement loss of the fundamental core modes [14]. In this paper, the effect of external hydrostatic pressure over the confinement loss in a side-hole mPOF (SH-mPOF) is studied and methods to tune the SPSM state are presented. The study was carried out in the visible region, where the PMMA is transparent [3]. By using a full-vector finite element method, the effective complex refractive index for the fundamental core modes and the cladding modes was calculated in order to determine the effect of the pressure over the confinement loss.

The results show that the SPSM regime can be obtained by applying external hydrostatic pressure for a fixed wavelength and that tuning the operation pressure is achievable by modifying the input wavelength. Finally, the effect of small changes in the fiber microstructure is considered.

II. Modeling

The change in the optical fiber characteristics occurs due to the photoelastic effect. The stress generated by pressure into the fiber induces anisotropy in the material refractive index, where the plane-strain approximation is assumed—in which the length of the fiber is much longer than any dimension of the waveguide cross section. The anisotropic refractive index has the form

$$n_x = n + C_1\sigma_x + C_2(\sigma_y + \sigma_z) \quad (1)$$

$$n_y = n + C_1\sigma_y + C_2(\sigma_x + \sigma_z) \quad (2)$$

$$n_z = n + C_1\sigma_z + C_2(\sigma_x + \sigma_y) \quad (3)$$

$$n_{xy} = (C_1 - C_2)\tau_{xy} \quad (4)$$

where n is the Sellmeier refractive index for the isotropic material, $C_1 = -5.0 \times 10^{-6}$ bar^{-1} and $C_2 = -4.8 \times 10^{-6}$ bar^{-1} are the stress-optic coefficients for PMMA, σ_x, σ_y, and σ_z are the normal stress components, and τ_{xy} is the shear stress. C_1 and C_2 coefficients were calculated by using the conventional analytical expressions for isotropic materials [15]. In these expressions, the following parameters were used for PMMA: Young's

Manuscript received December 17, 2010; revised April 08, 2011; accepted May 12, 2011. Date of publication May 27, 2011; date of current version July 27, 2011. This work was supported by the Brazilian agencies Capes (Pro-Defesa), Fapesp, CNPq (Fotonicom), and Finep.

Y. A. V. Espinel and C. M. B. Cordeiro are with the Institute of Physics, State University of Campinas, Sao Paulo, Brazil (e-mail: alexespi@ifi.unicamp.br; cmbc@ifi.unicamp.br).

M. A. R. Franco is with the Institute of Advanced Studies, Sao Paulo, Brazil, and also with the Institute of Technology of Aeronautics, Sao Paulo, Brazil (e-mail: marcos@ieav.cta.br).

Color versions of one or more of the figures in this paper are available online at http://ieeexplore.ieee.org.

Digital Object Identifier 10.1109/JLT.2011.2157893

0733-8724/$26.00 © 2011 IEEE

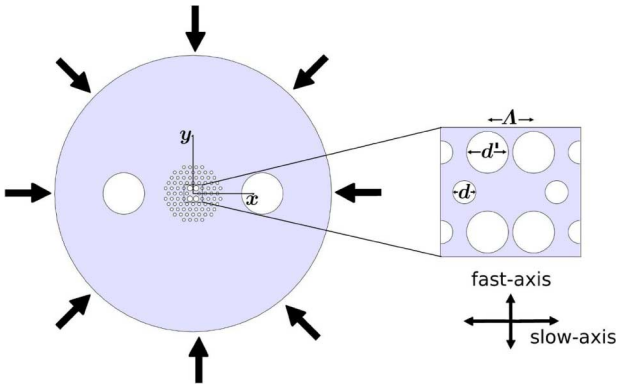

Fig. 1. SH-mPOF cross section and zoom of the core area. Geometrical parameters are: $\Lambda = 4.4\ \mu$m, $d = 2.2\ \mu$m and $d' = 4.0\ \mu$m, side-hole diameter is 30 μm, external diameter is 200 μm, and separation from each side hole to the fiber centre is 50 μm. Radial arrows indicate the applied hydrostatic pressure.

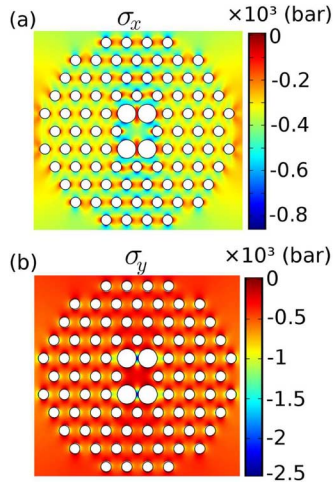

Fig. 2. Stress components induced for $p_{\text{ext}} = 380$ bar. (a) σ_x. (b) σ_y.

modulus, E = 3.2 GPa; Poisson's ratio, $\nu = 0.34$; photoelastic coefficients, $p_{11} = 0.300$ and $p_{12} = 0.297$ [16]. To model this problem, a commercial full-vectorial finite element software was used. The optical and mechanical effects were coupled with this program by using the structural mechanics and radio frequency package modules.

The structural mechanics module solves the equilibrium equations, $-\nabla \cdot \sigma = \boldsymbol{F}$. Here, the stress tensor σ is assumed, for isotropic materials, to be linearly dependent to the strain, being its dependence related to the elasticity matrix, and $\boldsymbol{F}$ denotes the volume forces that in this case are assumed to be null. The radio frequency module, on the other hand, implements the vectorial propagation equations for both $\boldsymbol{E}$ and $\boldsymbol{H}$ fields. In addition, a special truncation technique is used, based on a circular perfectly matched layer, surrounding the microstructured cladding in order to allow calculating the imaginary part of the effective refractive index related to the confinement loss [17].

III. Results

The proposed SH-mPOF is shown in Fig. 1 and has the following geometrical parameters: separation between holes (pitch), $\Lambda = 4.4\ \mu$m—constant across the microstructure, diameter of the bigger and the smaller holes, 4.0 and 2.2μm, diameter of the two large air channels (side holes) and the separation from each one to the fiber center, 30 and 50 μm, respectively. The arrows in the figure represent the applied hydrostatic pressure. It should be noted that the microstructure is not significantly deformed in the pressure range studied here and, as a consequence, the confinement loss is not drastically modified due to the slight geometric change. The modal birefringence, for example, changes less than 1% when the deformation is taken into account—and so, to simplify the model, was not considered here.

The fiber has a simulated phase birefringence $B_p = 3.1 \times 10^{-5}$ for $\lambda = 588$ nm when no pressure is applied. In addition, the sensitivity of the phase modal birefringence to the hydrostatic pressure dB_p/dP at the same wavelength is low, 0.75×10^{-6} MPa^{-1}, in contrast to other side-hole fibers [18], [19], where dB_p/dP can achieve 10^{-5} MPa^{-1}.

To evaluate the SPSM operation it was necessary to estimate the polarization extinction ratio (PER) defined as [20]

$$\text{PER}\ (dB) = -10 \log \left(\frac{T_{\text{fast}}}{T_{\text{slow}}} \right) \tag{5}$$

where T_{fast} and T_{slow} are the transmitted optical power of the fast- and slow axis modes (see Fig. 1), respectively.

By using of the definition of the PER in (5) and the definition of the loss (attenuation), it is possible to demonstrate also that

$$\text{PER} = P_{\text{FM}-y} - P_{\text{SM}-x}, \tag{6}$$

where $P_{\text{FM}-y}$ and $P_{\text{SM}-x}$ are the confinement losses of core modes [see Fig. 5(a)]. To carry out the simulation ∼110 000 second order triangular vector elements were used for the meshing of the fiber cross section and, as a result, about one million degrees of freedom were obtained.

The induced stress in the fiber cross section for an applied pressure of 380 bar is shown in Fig. 2. It can be noted that the stress component σ_x [see Fig. 2(a)] is lower than the stress component σ_y [see Fig. 2(b)] because the side holes (placed in the *x*-axis) reduce the load along the *x*-axis, but increase in the *y*-axis.

The variation of the material refractive index, (1)–(3), due to the modeled values of the stress components (typical results in Fig. 2), changes the effective refractive index of the fiber core and cladding modes. Fig. 3 shows the behavior of these indexes as a function of pressure. As the SH-mPOF is single mode at the wavelength range used in this paper, the core modes are represented as the fast- and slow axis modes (see Fig. 1), and are denoted by FM-*y* (*y*-polarized) and SM-*x* (*x*-polarized), respectively. In the cladding, we have the fundamental space-filling modes (FSM) [21] (*x*- and *y*-polarized) and, the cladding low-order modes that are denoted as CL_{21} (*x*- and *y*-polarized), where the subscripts 2 and 1 indicate the number of the dominant electric field extremes along of the *x*- and *y*-axes, respectively. These fields are symmetrical with respect to the *y*-axis.

As can be seen from Fig. 3, the effective indexes are, in all cases, enhanced by pressure because the material refractive index increases with pressure. The cladding effective in-

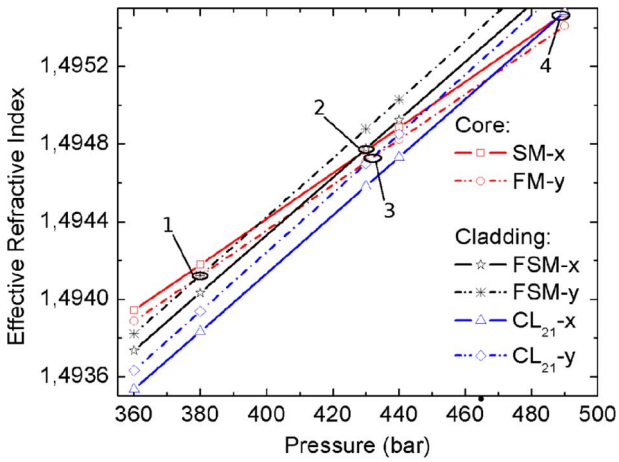

Fig. 3. Core and cladding effective refractive indexes as a function of hydrostatic pressure. The FM-y and SM-x modes (red lines) represent the fast- and slow axis modes, respectively; the FSM modes (black lines) represent the FSM (x- and y-polarized), and CL_{21} modes (blue lines) represent the cladding low-order modes(x- and y-polarized). The labels 1 to 4 show, for $\lambda = 588$ nm, the PMC between the core and cladding modes with the same polarization occurring for different pressures.

dexes, however, increase at a higher rate. This index enhancing is related to (1) and (2): the applied pressure induces a negative stress (see Fig. 2) that is multiplied by a negative factor (stress-optic coefficients). Due the different rates of the core and cladding modes enhancement, a phase-matched condition (PMC) is obtained—labels 1, 2, 3, and 4—when the effective core and cladding mode indexes become equal.

The different rates of the core and cladding modes that change with the applied pressure (see Fig. 3) are related to how the stress is distributed in the core and cladding regions. As expected from Fig. 1, the core experiences a diminishing in the stress components (σ_x and σ_y) as it is surrounded by four bigger holes in the first ring (y-axis), and the side holes in the x-axis. The cladding modes sensitivity to pressure, on the other hand, is only influenced in the x-direction by the side holes. As a result, the cladding modes suffer stronger influence than the core ones.

In addition, it can be noted that the modal birefringence of the core modes is maintained almost constant for this pressure range being twice the value when the pressure is null. In the case of the FSM modes, the modal birefringence is approximately 9.5×10^{-5} for the same pressure range and around 10^{-6} when no pressure is applied. Therefore, the sensitivity of the FSM mode is larger than the sensitivity of the core mode.

To clarify the influence of the side holes in the fiber characteristics and to better show that the coupling in the y-direction happens for lower pressures than the coupling in the x-direction (see labels 1 and 2 in Fig. 3), the fiber refractive indexes are presented. Fig. 4 shows the changes in the material refractive index for $\lambda = 588$ nm and $p_{\mathrm{ext}} = 380$ bar. Fig. 4(a) shows the changes in the n_x refractive index (Δn_x). Δn_y is not shown but have almost the same values due to the very similar stress-optic coefficients for PMMA (1) and (2). Fig. 4(b) and (c) shows the changes in the refractive index (Δn_x and Δn_y) for the x-axes [see Fig. 4(a)] and y-axes [see Fig. 4(b)]. The gray areas represent the cladding holes regions (air).

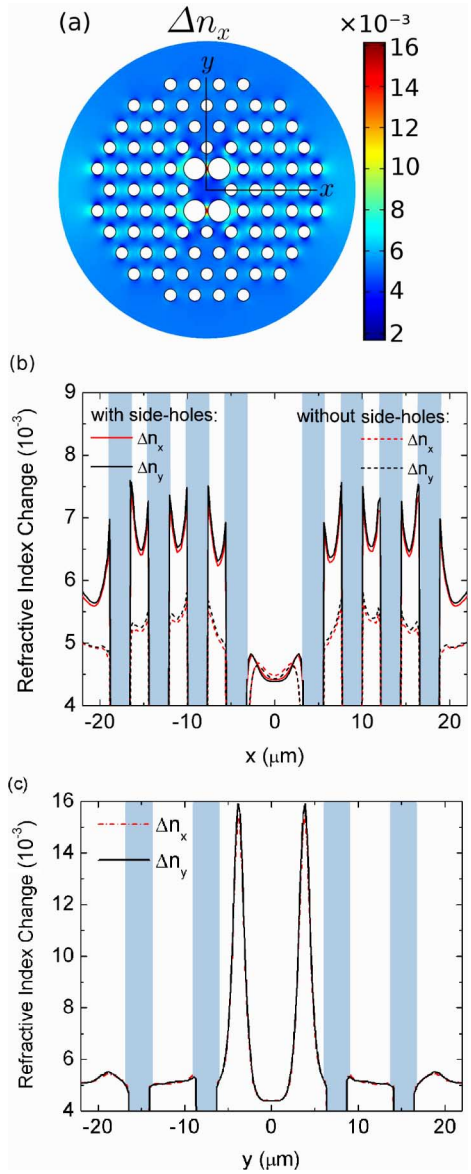

Fig. 4. Refractive index change across the fiber cross section for $\lambda = 588$ nm and $p_{\mathrm{ext}} = 380$ bar. (a) Δn_x. (b) Δn_x and Δn_y across the x axis for a fiber with (solid lines) and without (dashed lines) the side holes. (c) Δn_x and Δn_y across the y axis for a fiber with the side holes. The shaded regions in figure (b) and (c) represent the air holes in the cladding ($\Delta n_x = \Delta n_y = 0$).

As noted in Fig. 4(b), the change in the material refractive index in the cladding region is higher than in the core as observed in Fig. 3. Also, the refractive index changes in the cladding region for the fiber with side holes (solid lines) are higher than the changes for the same fiber but without the side holes (dashed lines), while in the core the values are similar.

In resume, the presence of the side holes means that the PMC of the core–cladding modes can occur at a lower applied pressure. To quantify this effect, the confinement loss was calculated: while it takes 380 bar to induce the first PMC in an SH-mPOF(label 1, Fig. 3), this value changes to 725 bar for the same fiber but without the side holes.

With a careful look in Fig. 4(b), it can also be observed that Δn_y is greater than Δn_x in the cladding while the opposite occurs in the core area meaning that the PMC of the core–cladding

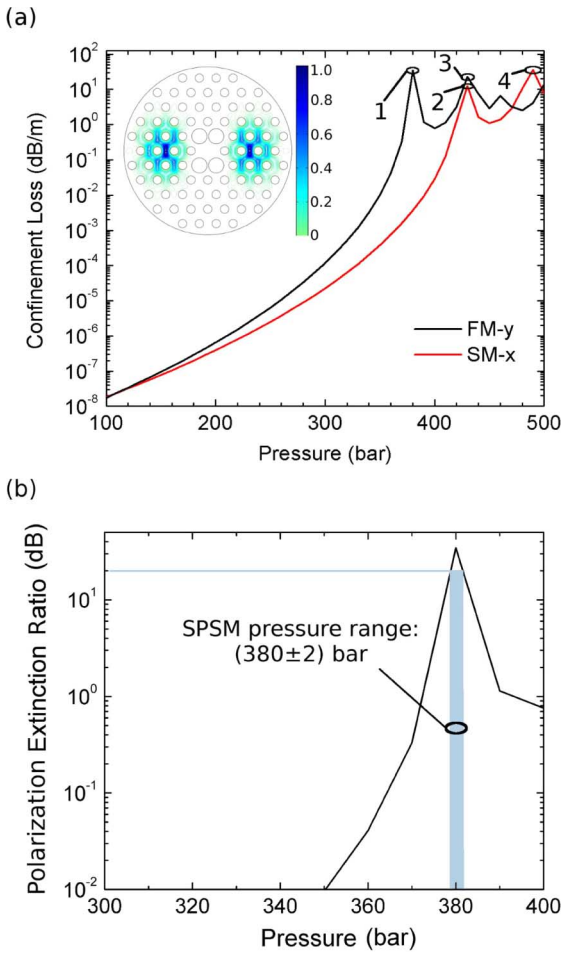

Fig. 5. (a) Confinement loss as a function of pressure for the core modes (x and y) for $\lambda = 588$ nm. The FM-y (black line) and SM-x (red line) modes represent the fast- and slow axis modes, respectively. Inset shows the normalized power flow in the z axis for the FSMs. (b)PER between the core modes.

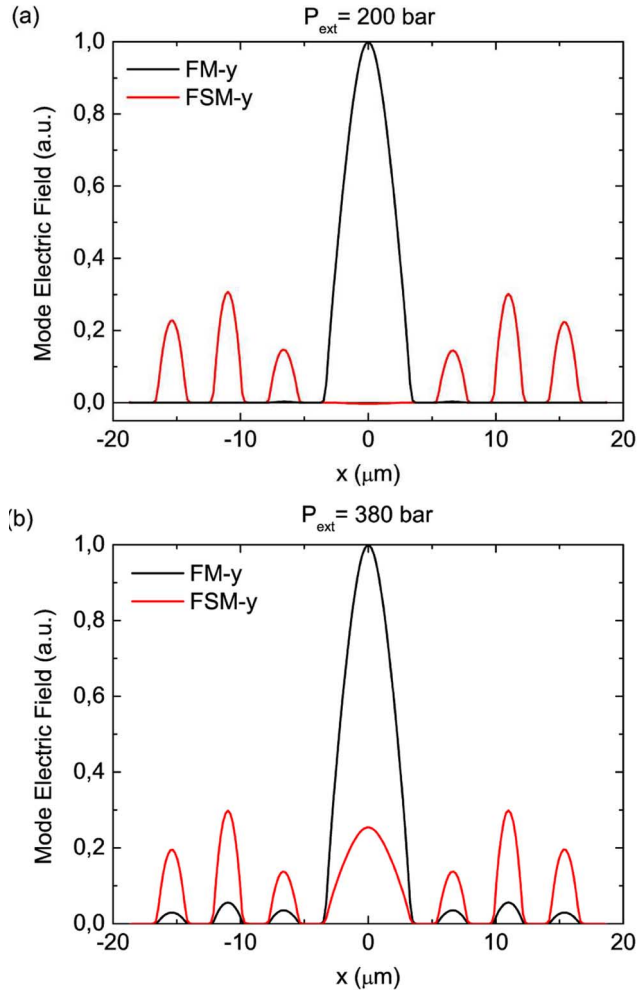

Fig. 6. Electric field's dominant components along to the x axis to the FM-y (black line) and FSM-y (red line) modes for (a) $p_{\rm ext} = 200$ bar and (b) $p_{\rm ext} = 380$ bar, for $\lambda = 588$ nm.

modes will occur first for y-polarized modes (label 1, Fig. 3). In Fig. 4(c) (y-axis), Δn_x and Δn_y do not show a significant difference for both core and cladding, apart from the two peaks that are related to the small gap between the holes with bigger diameter (d', Fig. 1), where the stress is greater as seen in Fig. 2.

To check how the confinement losses of the x- and y-core modes evolve with the applied pressure, its values are plotted for $\lambda = 588$ nm and are shown in Fig. 5(a). Here, the variation of the confinement loss is related to the coupling between the core and cladding modes. Initially, the confinement loss increases up to a maximum value (see Fig. 5(a), labels 1 and 2). At low pressures [e.g., 200 bar, Fig. 6(a)], the electric fields of the core (solid line) and cladding (dashed line) modes are in different regions, meaning a weaker spatial overlap and small coupling. As a consequence, a low confinement loss is expected. Fig. 5(a) shows the z-component of the normalized power flow of the cladding mode—as noted, at low pressures it is confined to the cladding region. At high pressures [e.g., 380 bar, Fig. 6(b)], on the other hand, a field component of each mode appears in the region of the other mode and, as a consequence, a stronger overlap and coupling between the modes happen.

The confinement loss is also dependent on the phase mismatch (difference between effective refractive indices) between core and cladding modes with same polarization (x or y). Label 1 in Fig. 3 shows the situation where the FM-y and FSM-y modes have the same refractive index. Fig. 5(b) shows the SPSM region (shaded region (380 ± 2) bar) where an extinction ratio greater than 20 dB was obtained. From Fig. 5(b), it can be noted that the PER enhances dramatically with pressure (in the range of 350–380 bar) ranging from 0.01 to 30 dB. Such strong sensitivity could be potentially used to develop a hydrostatic pressure sensor.

The periodic behavior of the confinement loss observed in Fig. 5(a), labels 3 and 4, is related to the coupling between the core and the CL_{12} cladding modes. This behavior is also found in the bending loss of curved photonic crystal fibers [22], [23].

A. Tuning the SPSM Regime

In the previous section, the SPSM regime was achieved for a fixed pressure of $p_{\rm ext} = 380$ bar. Here, the possibility to get the SPSM regime in other pressures, if the operation wavelength is modified, will be shown.

The spectral dependence of the confinement loss for different hydrostatic pressures (330, 380, and 430 bar) are presented in Fig. 7. The peaks in each figure represent the PMC coupling

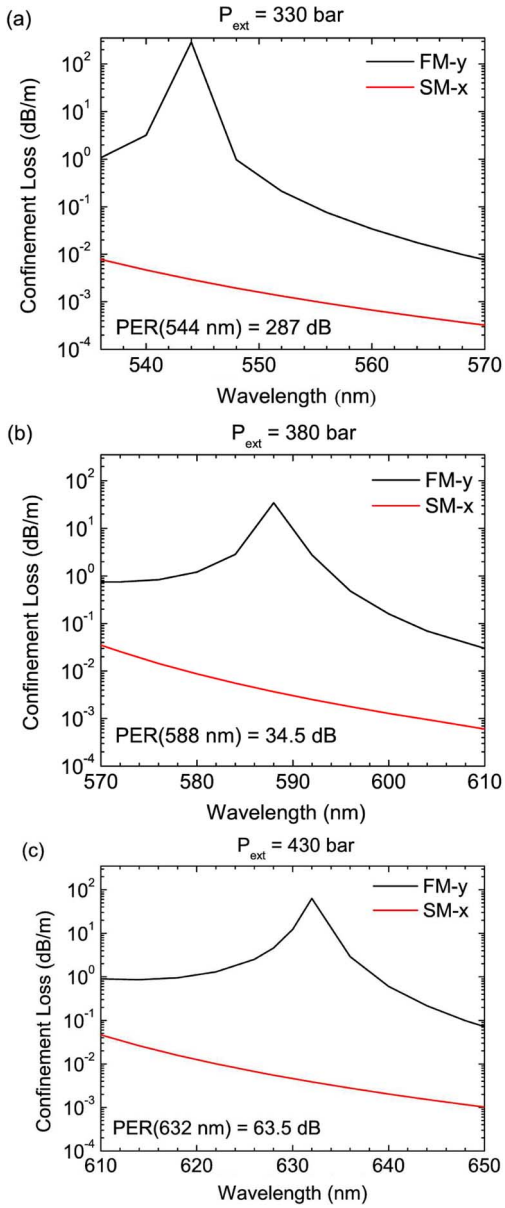

Fig. 7. Confinement loss as a function of wavelength for the core modes for the hydrostatic pressures. (a) $p_1 = 330$ bar. (b) $p_2 = 380$ bar. (c) $p_3 = 430$ bar. The peaks are related to the PMC between the FM-y and FSM-y modes. PER values also presented at operation wavelength.

between the FM-y and FSM-y modes (the peak in Fig. 7(b), in particular, is related to label 1 in Fig. 3). As noted the PMC occurs, for each pressure, in a different operation wavelength: $\lambda_1 = 544$ nm ($p_1 = 330$ bar), $\lambda_2 = 588$ nm ($p_2 = 380$ bar) and $\lambda_3 = 632$ nm ($p_3 = 430$ bar). Therefore, if the input wavelength increases, then this should occur with the applied pressure to get the SPSM regime.

It is possible to observe that, for each operation wavelength, the confinement loss for the SM-x and FM-y modes is around 10^{-2} dB/m and 10^{2} dB/m, respectively. Very high PER of about 287 dB at $\lambda_1 = 544$ nm could be reached when 330 bar of hydrostatic pressure was applied to the mPOF. Considering $\mathrm{PER} > 20$ dB as a limitrophe SPSM condition, it is possible

TABLE I
MAXIMUM POLARIZATION EXTINCTION RATIO (PER) TO SM-X AND FM-Y CORE MODES AND BANDWIDTH (PER$>$ 20 DB)

P_{ext} (bar)	λ (nm)	PER (dB)	Bandwidth $\Delta\lambda$ (nm)
330	544	~287	10
380	588	~34.5	10
430	632	~63.5	12

to determine the bandwidth $\Delta\lambda$ of SPSM operation. The maximum PER and the spectral operational range are summarized in Table I.

B. Influence of the Geometry in the SPSM Regime

It could be desirable to tune the SPSM regime to smaller pressures in order to reduce stress points within the fiber structure, keeping the operation wavelength fixed.

To accomplish this, a fiber with slight structural modification from the one shown in Fig. 1 was studied. The approach was based on changing the structure in order to modify the form birefringence, without drastically changing the birefringence of the FSM, and then anticipating the PMC coupling for smaller pressures.

The inset of Fig. 8(a) shows the new geometry that consists in changing the position of the four bigger holes that surround the core and reducing the size of the two other holes that complete the core area. The original geometry is marked in black while the new one in gray: the position of these four holes changed by 0.5 μm in the direction to the fiber center while the two extra holes changed from 2.2 to 1.8 μm in diameter. The new geometry reduces the core effective refractive indexes and increases the phase modal birefringence (7×10^{-5}) with respect to the initial value $(B_p = 3.1 \times 10^{-5})$ for $p_{\mathrm{ext}} = 0$ bar and $\lambda = 588$ nm. As the new configuration only affects the inner ring slightly, the FSM maintaining the effective refractive indexes is almost unmodified.

It is important to note that mPOF are in general produced by drilling holes in a solid acrylic rod [3] which means that, in contrast with the stacking and draw technique widely used to produce silica photonic crystal fibers [1], [2], the holes position can be chosen with high freedom.

As a result it can be seen in Fig. 8, for $\lambda = 588$ nm, that the PMC coupling (label 1) happens, as expected, to lower pressures (100 instead of 380 bar). In addition, the confinement loss for the SM-x and FM-y modes are around of 2×10^{-2} and 38.8 dB/m, respectively, resulting in a PER of 38.8 dB ($\Delta\lambda = 15$ nm), within the typical values presented in Table I, but with the advantage of reducing the operation pressure to ~26% of the originally calculated value (see Fig. 5). The coupling of the core–cladding x-polarized modes also suffered a strong reduction going from 430 (see Fig. 5(a), label 2) to 135 bar (see Fig. 8(a), label 2). Apart from reducing the operation pressure, an extra advantage of this new geometry relates with the reduction of the built-in high-stress regions. While the region between each pair of larger holes that surround the core area has a stress as high as 2500 bar [see Fig. 2(b)], the new geometry reduces this value to 640 bar.

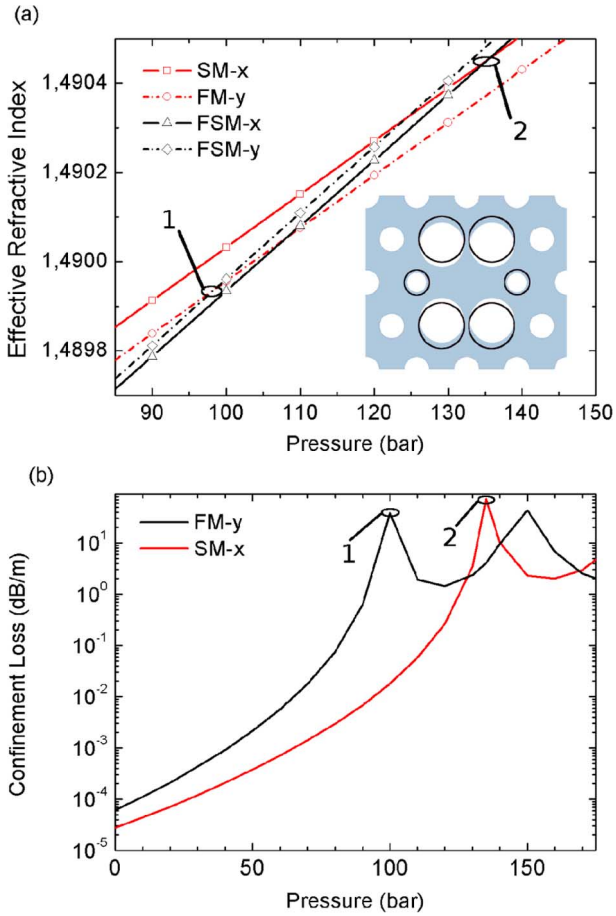

Fig. 8. (a) Effective refractive indexes for the core and FSM modes as a function of pressure for the modified fiber (inset). Inset shows the core area of both original (black rings) and modified fiber (gray). (b) Confinement loss of the core modes calculated at $\lambda = 588$ nm as a function of pressure for the modified fiber.

IV. Conclusion

An mPOF with side holes was proposed where the SPSM regime is induced by pressurizing the fiber hydrostatically. The external pressure induces anisotropic stress in the fiber cross section and works as a controllable optical loss mechanism that is related to the coupling between core and cladding modes. It was found that, in PMMA, the operation pressure is in the range of 10^2 bar. Two methods were proposed for tuning the SPSM regime: 1) modifying the operational wavelength, and 2) taking advantage of the design freedom of mPOF, in particular for fibers manufactured by the drilling process (polymeric ones), to change the geometry slightly in order to play with the core birefringence and the effective refractive indexes of the core modes. The second approach allows reducing the applied pressure, with the extra advantage of alleviating mechanically the structure, and to keep the wavelength fixed.

Finally, as a consequence, this kind of device can be used as a tunable polarizing element with potential use in optical communication systems and, also, as a pressure sensor.

References

[1] P. Russell, "Photonic crystal fibers," *Science*, vol. 299, no. 5605, pp. 358–362, 2003.

[2] J. C. Knight, "Photonic crystal fibers," *Nature*, vol. 424, pp. 847–851, 2003.

[3] M. Large, L. Poladian, G. Barton, and M. A. van Eijkelenborg, *Microstructured Polymer Optical Fibres*, 1st ed. Sydney, Australia: Springer-Verlag, 2008.

[4] J. C. Baggett, T. M. Monro, K. Furusawa, V. Finazzi, and D. J. Richardson, "Understanding bending losses in Holey optical fibers," *Opt. Commun.*, vol. 227, no. 4–6, pp. 317–335, 2003.

[5] G. Statkiewicz, T. Martynkien, and W. Urba'nczyk, "Measurements of modal birefringence and polarimetric sensitivity of the birefringent Holey fiber to hydrostatic pressure and strain," *Opt. Commun.*, vol. 241, no. 4–6, pp. 339–348, 2004.

[6] T. Martynkien, M. Szpulak, and W. Urbanczyk, "Modeling and measurement of temperature sensitivity in birefringent photonic crystal Holey fibers," *Appl. Opt.*, vol. 44, no. 36, pp. 7780–7788, 2005.

[7] M. C. J. Large, D. Blacket, and C.-A. Bunge, "The role of viscoelastic properties in strain testing using microstructured polymer optical fibres (mpof)," *Meas. Sci. Technol.*, vol. 20, no. 3, p. 034014, 2009.

[8] M. K. Szczurowski, T. Martynkien, G. Statkiewicz-Barabach, W. Urba'nczyk, and D. J. Webb, "Measurements of polarimetric sensitivity to hydrostatic pressure, strain and temperature in birefringent dual-core microstructured polymer fiber," *Opt. Exp.*, vol. 18, no. 12, pp. 12076–12087, 2010.

[9] K. Saitoh and M. Koshiba, "Single-polarization single-mode photonic crystal fibers," *IEEE Photon. Technol. Lett.*, vol. 15, no. 10, pp. 1384–1386, Oct. 2003.

[10] A. D. J. L. C. M. Delgado-Pinar, and M. V. Andrés, "High extinction ratio polarizing endlessly single-mode photonic crystal fiber," *IEEE Photon. Technol. Lett.*, vol. 19, no. 8, pp. 562–564, Apr. 2007.

[11] R. Li-Yong, W. Han-Yi, Z. Ya-Ni, Y. Bao-Li, and Z. Wei, "Theoretical design of single-polarization single-mode microstructured polymer optical fibres," *Chin. Phys. Lett.*, vol. 24, no. 5, pp. 1298–1301, 2007.

[12] Y.-N. Zhang, "Design of low-loss single-polarization single-mode photonic-crystal fiber based on polymer," *J. Mod. Opt.*, vol. 55, no. 21, pp. 3563–3571, 2008.

[13] D. A. Nolan, M.-J. Li, X. Chen, and J. Koh, "Single polarization fibers and applications," presented at the Opt. Fiber Commun. Conf. (Opt. Soc. Amer.), Washington, DC, 2006, no. OWA1.

[14] Y. A. V. Espinel, M. A. R. Franco, and C. M. B. Cordeiro, "Pressure induced single-polarization single-mode microstructured polymer optical fiber," presented at the Latin Amer. Opt. Photon. Conf. (Opt. Soc. Amer.), Washington, DC, 2010, no. WE27.

[15] M. J. Weber, *CRC Handbook on Laser Science and Technology, Supplement 2: Opticals Materials*, 1st ed. Boca Raton, FL: CRC Press, 1995.

[16] R. M. Waxler, D. Horowitz, and A. Feldman, "Optical and physical parameters of plexiglas 55 and lexan," *Appl. Opt.*, vol. 18, no. 1, pp. 101–104, 1979.

[17] X. Chen, M.-J. Li, J. Koh, A. Artuso, and D. A. Nolan, "Effects of bending on the performance of hole-assisted single polarization fibers," *Opt. Exp.*, vol. 15, no. 17, pp. 10629–10636, 2007.

[18] H. M. Xie, P. Dabkiewicz, R. Ulrich, and K. Okamoto, "Side-hole fiber for fiber-optic pressure sensing," *Opt. Lett.*, vol. 11, no. 5, pp. 333–335, 1986.

[19] M. Szpulak, T. Martynkien, and W. Urbanczyk, "Highly birefringent photonic crystal fibre with enhanced sensitivity to hydrostatic pressure," in *Proc. 8th Int. Conf. Transparent Opt. Netw. 5th Eur. Symp. Photon. Cryst.*, 2006, vol. 4, pp. 174–177.

[20] D. Penninckx and N. Beck, "Definition, meaning, and measurement of the polarization extinction ratio of fiber-based devices," *Appl. Opt.*, vol. 44, no. 36, pp. 7773–7779, Dec. 2005.

[21] T. A. Birks, J. C. Knight, and P. S. Russell, "Endlessly single-mode photonic crystal fiber," *Opt. Lett.*, vol. 22, no. 13, pp. 961–963, 1997.

[22] G. C. Balvedi and M. A. R. Franco, "Effect of coupling between fundamental and cladding modes on bending losses in single-polarization single-mode photonic crystal fiber," in *Proc. Amer. Inst. Phys. Conf.*, 2008, vol. 1055, no. 1, pp. 137–140.

[23] J. Olszewski, M. Szpulak, and W. Urba'nczyk, "Effect of coupling between fundamental and cladding modes on bending losses in photonic crystal fibers," *Opt. Exp.*, vol. 13, no. 16, pp. 6015–6022, 2005.

Yovanny A. V. Espinel was born in Bogotá, Colombia, in July, 1981. He received the B.Sc. degree in physics from the National University of Colombia, Bogota, in 2007. He is currently working toward the master's degree from the State University of Campinas, Sao Paulo, Brazil and a Researcher at the National Institute of Science and Photonics Technology for Optical Communications, Sao Paulo, Brazil.

His main research interests include computational physics, photonic crystal fibers, tapers, and fiber optic sensors

Marcos A. R. Franco was born in Santo André-SP, Brazil, in June, 1962. He received the B.S. degree in physics from the Pontifical Catholic University, São Paulo, Brazil, in 1983, the M.S. degree in physics from the University of São Paulo, São Paulo, in 1991, and the Ph.D. degree in electrical engineering from the University of São Paulo, in 1999.

He is currently a Researcher at the Institute of Advanced Studies (IEAv), São José dos Campos-SP, and a Professor at the Institute of Technology of Aeronautics, São José dos Campos-SP, in the postgraduate program of Electronics and Computer Engineering. He is also the Coordinator of the Computational Electromagnetic Laboratory at IEAv. His main research interests include applied electromagnetic, computational modeling of electromagnetic devices, optical fibers, fiber optic sensors, integrated optics, photonic crystal fibers, microstructured optical fibers, wave propagation, microwave, and finite element method.

Cristiano M. B. Cordeiro received the Ph.D. degree from the Institute of Physics of the State University of Campinas (UNICAMP), Campinas, Brazil, and the Postdoctoral Researcher from the University of Bath, England.

He is currently a Professor at the Institute of Physics, UNICAMP. He is the head of the Specialty Optical Fiber & Photonics Materials Laboratory at UNICAMP. His main research interests include the development and application of photonic crystal fibers and micro/nanofibers, and the waveguide structural and material postprocessing for exploring new fiber functionalities. Applications related to optical devices and sensors, telecommunications, and nanophotonics are under investigation.